Load-Sharing in Soft and Spiny Paws for a Large Climbing Robot

Wilson Ruotolo, Frances S. Roig, and Mark R. Cutkosky

***Abstract*—A novel end-effector is presented for a large climbing robot. The gripping surfaces are covered with sharp spines to achieve a high shear stress on rocky surfaces. Soft, flexure-based joints and the natural compliance of a particle-jamming pad in the palm allow the end-effector to conform to a variety of shapes without complex controls, while strong tendons and the application of vacuum to the palm create rigidity when applying loads of 250 N and greater. A differential mechanism distributes the force from a single actuator to the phalanges of the fingers, providing approximately equal tangential forces at each contact. The particle-jamming palm allows many spines to contact a rough surface, then becomes nearly rigid so that they share the load. Tests on instrumented surfaces confirm the predicted load-sharing of the fingers and performance of the palm.**

***Index Terms*—Biomimetics, compliant joint/mechanism, tendon/wire mechanism.**

I. Introduction

AN ENDURING challenge for legged robots is to negotiate steep, rocky surfaces that might be encountered in planetary exploration or in search and rescue situations. In such applications, large robots have the advantage of being able to step over correspondingly large obstacles and gaps while carrying heavy payloads. However, they also impose particular challenges in designing the hands or feet, as the robot's weight grows with length cubed, while contact area grows with length squared. Humans and bears make up for this scaling law with intelligent hold selection, dynamic movements, and a rich set of sensor feedback, all of which are difficult for current robots to match.

Spines are a promising technology in this context, as they permit high shear stresses with little or no normal force [1]. A number of climbing robots have used claws or arrays of miniature spines to climb steep and even vertical rough surfaces [1]–[13]. However, these examples are relatively small (under 10 kg) and demonstrations have mostly been confined to structured surfaces like building walls or telephone poles. Other solutions involving suction or magnetic attraction have been demonstrated since the late 1980s for robots of 10–100 kg (e.g., [14]) but these again are restricted to man-made surfaces.

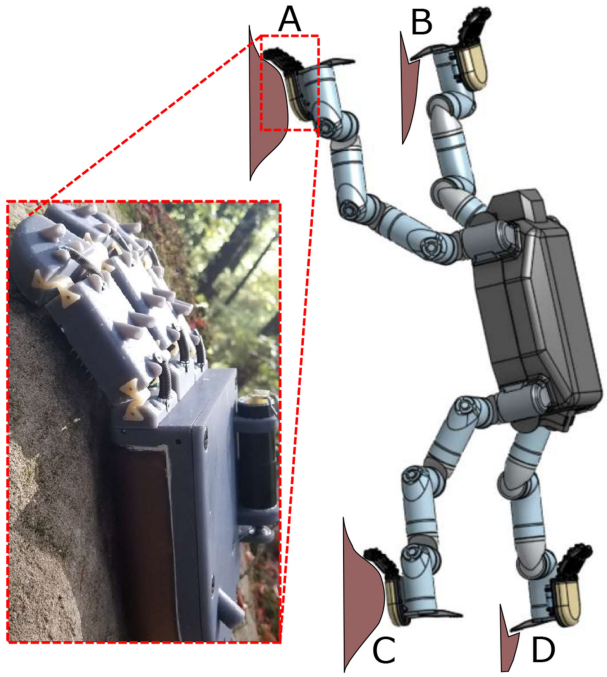

Fig. 1. RoboSimian uses the final roll joint in each limb to bring either a climbing hook (B, D) or soft and spiny end-effector (A, C) into play. Inset shows end-effector prototype gripping a rock.

In the present case we are interested in allowing a large, legged robot, RoboSimian [15], to climb steep, rocky surfaces such as cliffs. The project is part of a collaboration among teams at Duke University, U.C.S.B. and Stanford and includes motion planning and end-effector design. As seen in Fig. 1, the robot has a rotational "roll" joint near the end of each 7 DOF limb, which it can rotate to use either hook tools adapted from human climbing aids (B, D) or soft and spiny end-effectors (A, C) as desired.

A. Contributions

In this letter we focus on a new end-effector design, highlighted in A in Fig. 1, that draws upon the technology of soft robotics as well as under-actuated hands. The end-effector, which we call a paw rather than a hand because it is not capable

Manuscript received October 15, 2018; accepted January 11, 2019. Date of publication February 1, 2019; date of current version February 15, 2019. This letter was recommended for publication by Associate Editor P. Valdivia y Alvarado and Editor K.-J. Cho upon evaluation of the reviewers' comments. This work was supported by the NSF Award IIS-1525889. The work of W. Ruotolo was supported by NSF GRF. *(Corresponding author: Wilson Ruotolo.)*

The authors are with the Department of Mechanical Engineering, Stanford University, Stanford, CA 94305 USA (e-mail: wruotolo@stanford.edu; francess@stanford.edu; cutkosky@stanford.edu).

This letter has supplementary downloadable multimedia material available at http://ieeexplore.ieee.org, provided by the author. This includes a short video, which demonstrates the functionality of the various hand components. The material is 43 MB in size.

Digital Object Identifier 10.1109/LRA.2019.2897002

of opposed grasps, uses spines for high shear forces at the contacts. A consequent materials challenge is to combine numerous hard and very sharp spines with soft materials and construction methods. Whenever structures of very disparate stiffness are combined, stress concentrations arise at their interface which can produce tearing or delamination [16]. Fortunately, as with the concept of spines for climbing, nature provides some inspiration for integrating hard, sharp spines in soft structures. In particular, the tongues of large cats (e.g., tigers) and penguins contain numerous sharp spines of hard keratinous material embedded in soft muscular tissue [17]. In both cases the spines are used for gripping meat and are subjected to significant forces. A closer look at how the spines are attached to the tongue reveals some design strategies: the spines are angled backward so that they catch and pull when ingesting prey but flatten when the tongue is extending, and they are anchored with structures below the tongue surface that help to distribute the load.

In Section III we present the design of compliant, spiny fingers driven by a common actuator, and the design of a palm with a particle-jamming bed, covered with sharp spines embedded in a fabric. We present models to predict the load-sharing capabilities of the finger and palm subsystems so that tangential forces are not concentrated on just a few spines. The work draws upon recent developments in linearly-constrained spines [18], reviewed briefly in the next section. In Section IV we present the results of experiments to measure the load sharing in the fingers and palm, and confirm that the results agree with the models presented in the previous section. In Section V we draw conclusions and discuss future work to integrate the new end-effectors with RoboSimian.

II. Related Work

The work presented here draws directly upon a few areas of related work: (i) linearly-constrained spines, (ii) under-actuated hands, and (iii) soft robotics.

A. Linearly-Constrained Spines

As noted in the Introduction, spines have been used for over a decade in climbing robots. However, for large robots a new approach is desired so that hands or feet do not become impractically large. Linearly-constrained spines [18] address this concern. They consist of dense arrays of spring-loaded straight spines that slide in channels. On hard, rough sufaces they more than make up in spine density what they sacrifice in terms of load-sharing between spines. The maximum load force per spine is described by a probability density function because both asperity distribution and asperity strength are stochastic. Calculations and empirical results suggest that the maximum number of spines in a dense array should be 40–60, beyond which the overall force grows little due to imperfect load-sharing. A 100×120 mm palm with 12 spine arrays and a load-sharing system was demonstrated to support over 700 N in shear on a vertical concrete surface. Smooth, hard surfaces will often entail decreased performance, but the problem scope of this project focuses on natural rock, which is generally comparable in roughness.

A prototype hand was constructed to combine the palm with under-actuated fingers for grasping curved surfaces [19]. It demonstrated excellent load-sharing among spine arrays but was not flexible enough to conform to irregular, doubly-curved surfaces and not robust enough for mounting at the extremities of RoboSimian. The new design presented here aims to overcome those limitations.

B. Under-Actuated Hands

Under-actuated hands have become a popular solution for mobile robots. They can adapt passively to a wide range of shapes and have lower weight, lower complexity and greater robustness than fully-actuated hands. There is an extensive literature, including texts devoted to under-actuated hands [20] and recent reviews [21], [22]. Much of the traditional grasping literature concerns the locations of contacts and the control of contact forces in the normal direction. However, in the present case we are primarily concerned with *tangential* forces at the contacts, because spines can sustain large tangential forces nearly independent of the corresponding normal force.

C. Soft Robotics

To increase conformability and robustness with respect to impacts, the design presented here adopts the materials and construction methods that have become popular for soft robotics [23], [24]. However, the climbing end-effectors also need to be selectively stiff when large loads are applied. Among the solutions used in soft robotics for this purpose are embedded fibers or tendons that greatly stiffen a structure when actuated, and beds of particles that lock up when a vacuum is applied. A survey of these approaches can be found in [25] and notable examples include [26]–[28]. As noted in the Introduction, a unique challenge is imposed by the desire to integrate hard, sharp spines into otherwise soft structures. Our solution to this problem is presented in Section III-A.

III. Design

The new design presented here is part of a system illustrated in Fig. 2 to enable RoboSimian to climb steep rocky surfaces.

A. Particle Jamming Palm

In comparison to the flat palm reported in [18], early field testing showed that it would be necessary for a palm to conform to surfaces with high rugosity, bringing many spines into contact with the surface. However, when a load is applied, the palm needs to become stiff so that the spines move as a unit and local stretching does not produce failures that propagate across the palm. Possible solutions include a low-temperature metal alloy that is either liquid or solid or, as in the present case, a particle-jamming system, similar to that employed in other conformal grippers (e.g., [26]–[28]).

However, integrating a soft particle-jamming system with hard, sharp spines presents challenges. The spines are 1mm diameter by 7mm long pieces of hardened tool steel, tapering to a point with ≈ 15 μm tip radius, whereas the skin that supports

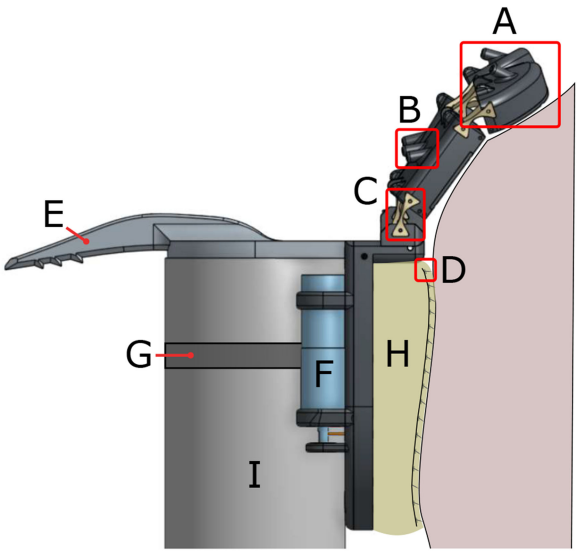

Fig. 2. System diagram and components: (A) Pneumatically actuated spiny phalanges (see Fig. 5). (B) Air inlets for spine chamber pressurization. (C) Soft flexure joints (see Fig. 4). (D) Cast spine unit (see Fig. 3). (E) Climbing tool inspired claw for positively angled wall features. (F) Motor for tendon actuation.(G) Final rotational joint of Robosimian arm. (H) Particle jamming palm chamber. (I) Robosimian arm.

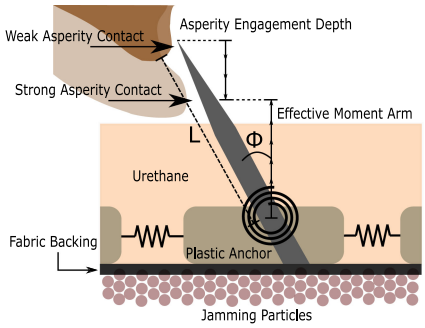

Fig. 3. Palm spine unit cross section and terminology.

them is a stretchy urethane of approximately 344kPa modulus. As they are loaded, embedded spines will tend to produce large local strains in the skin, leading to vacuum leaks and possibly tearing it. As noted in the Introduction, a similar problem is faced by animals with spiny tongues.

A solution, shown in Fig. 3, is to first embed the base of each spine in a $2 \times 4 \times 7$ mm anchor of intermediate hardness (Smooth On Task 9, 85D Shore). These anchors are bonded to a coated nylon fabric (ProSoft Waterproof 1 mil PUL) that supports the urethane skin. The spine units and fabric are arrayed in a two-part mold, and a 5 mm thick layer of urethane (Smooth On, Vytaflex 20, Shore 20A hardness) is cast into the shape of the palm outer surface. This distributes normal and shear forces to prevent perforations of the urethane skin under heavy loads.

As noted in [1], there are three primary failure modes for a spine asperity contact: plastic deformation of the spine tip, asperity breakage, and elastic rotation of the spine off of the asperity. The first has a very high force value ($\sim$40N) but forces on the order of tens of newtons should be avoided if possible because they quickly result in dulling of the spine tip [18]. The second failure mode is highly variable due to the stochastic nature of asperity distributions, and is not strongly affected by design choices other than tip diameter. The third, elastic rotation and slip-off, is an element that should be tuned for best performance.

Given that many spines find asperities upon initial contact [29], peak shear forces in the palm design are achieved just before those spines rotate off of their respective asperities. If the system is too stiff, many of those spines will undergo asperity breakage before translating far enough for other spines to engage.

If the system is too compliant, those initial contact spines rotate off before achieving their load potential. Consequently, the conditions for best performance are that the expected value of elastic spine force at the rotational limit equals the expected value of asperity failure, $E[F_{asperity}]$:

$$E[F_{asperity}] \approx E[(d_{travel} - d_{asperity})K_e] = E[F_{spine}] \quad (1)$$

where d_{travel} is the distance the palm travels, $d_{asperity}$ is the interval between asperities and K_e is the effective stiffness due to a combination of rotational and linear compliance, as shown in Fig. 3.

It was shown in [30] that asperity density can be described as:

$$P(D_{asperity} = d) \approx (1 - \alpha)\delta(d) + \alpha\lambda e^{-\lambda d} \quad (2)$$

where α represents the probability that the spine does not immediately engage with an asperity on contact and depends on spine travel and surface properties. For roofing shingle coated with small rock particles, as used in tests in Section IV-A, a reasonable value from [30] is $E[D_{asperity}] = \alpha/\lambda = 0.73/0.33$. Therefore, the following substitutions can be made:

$$E[F_{asperity}] \approx (L \sin\phi - \alpha/\lambda)K_e \quad (3)$$

If the surface spine contact properties of $E[F_{asperity}]$ and λ are known, the urethane material and geometric choices should determine L, ϕ and K_e such that the condition above is met. A finite element model using SimScale predicts a urethane embedded tile unit to have a K_e of 2.12 N/mm, so $L \approx 6$ mm (tip of spine to center of rotation) and $\phi \approx 40^\circ$ (25° of initial angle plus 15° past perpendicular to fully rotate off) are reasonable values to give an estimated failure force per spine of 3.5 N which is similar to the asperity failure values for many tested surfaces [1], [18].

In addition, it is visibly apparent under vacuum that deformations in the urethane skin (which remains bonded to the spines during deformation) dominate the compliance of the system, rather than shifting of the jammed particle substrate. This compliance allows passive load sharing to occur. If load sharing were perfect (spine rotation completely decoupled across the palm) then the anticipated maximum shear force would be approximately equal to $n \times E[F_{spine}] \approx 248$ N where $n = 71$ is the number of spines. We note also that the effective stiffness of each spine contact is proportional to the engagement depth (see Fig. 3). As noted in previous work, asperity strength grows roughly with the square of asperity size [18], which means that the system is designed to allocate higher forces to the stronger,

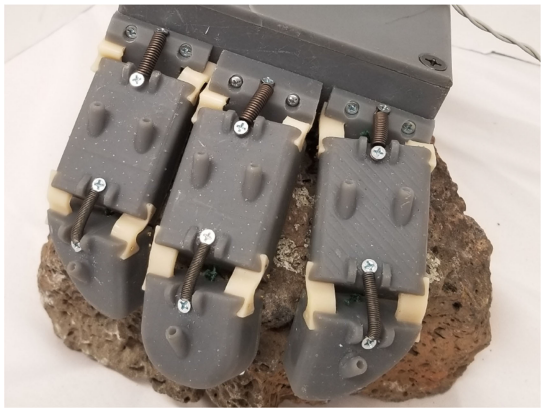

Fig. 4. Flexures allow passive conformation in bending and twist. Tendons through the joints support the large contact forces.

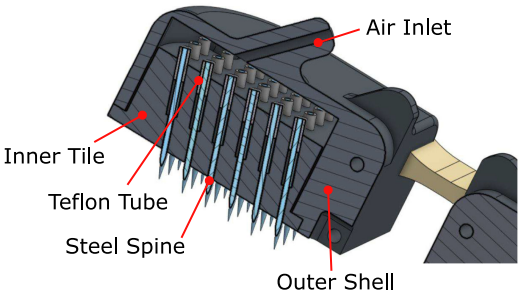

Fig. 5. Pneumatic spine array cross section.

larger asperities, leaving potential for improved shear force beyond this value. In practice, load sharing is imperfect and the actual maximum force over the palm is closer to half this value as described in Section IV-B.

B. Fingers With Spines

The palm allows a high shear force over a compact area. However, on rounded features, human climbers can support higher loads using their fingers to partially envelop the feature in a "sloper" grip [31]. To emulate this capability we equip the end-effector with three fingers (Fig. 4), which are also equipped with spines.

Each phalange functions similarly to a single dense spine array, as described in [18], with 50 spines in distal phalanges and 56 in proximal phalanges. Instead of miniature springs, a 0.34 bar pneumatic pressure extends the spines, as shown in Fig. 5. Teflon sleeves allow the spines to slide smoothly while minimizing air leakage. This solution is much easier to assemble than the previous spine arrays and allows a lower normal force to push the spine array against a surface. The air also helps to prevent small particles from jamming the spines.

C. Finger Actuation and Load Sharing

The spine tiles in the fingers create a series of phalanges with soft, elastomeric flexures at the joints. The flexures, and additional coil springs on the dorsal surfaces, stabilize the fingers when they are unloaded. However. when grasping a surface, the main load forces are parallel to the phalanges and are supported by internal tendons.

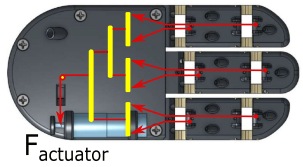

Fig. 6. Whiffle tree load sharing system. Tendon force ratios (here shown equal) can be specified by varying the beam lengths.

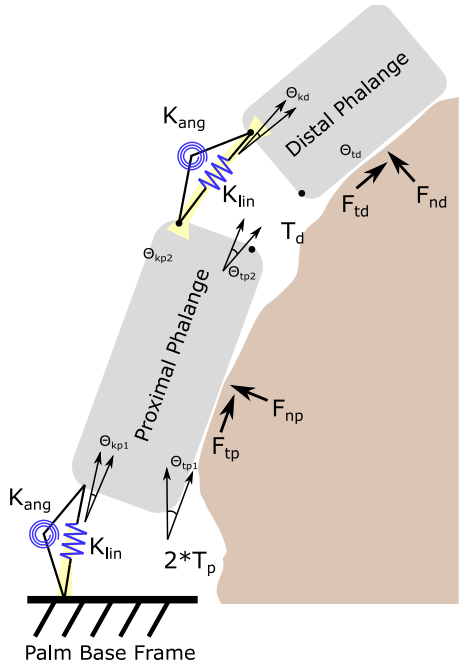

Fig. 7. Phalange loading force diagram: K_{ang} and K_{lin} represent flexure stiffness, T_p and T_d are tendon forces.

The system here differs somewhat from the usual paradigm in designing under-actuated hands where tendon routing and pulley diameters are chosen to achieve a desired distribution of normal forces as the fingers close upon a range of object shapes. Here, the normal forces are relatively unimportant because the spines can produce large shear forces almost independent of the normal force. Instead, we wish to specify tangential forces at the contacts.

Figures 6 and 7 illustrate the load-sharing approach. Each finger has two tendons routed over smooth steel dowel pins and anchored to the midpoint of the structure, as close to the contact surface as possible. In this way, loads from the spine arrays are transferred directly to the tendons, without producing bending moments that could dislodge the contact.

The tendons are linked to a single motor via a six-way whiffle tree in the rigid part of the palm structure (Fig. 6), creating a differential system that ensures even forces on the tendons. Note that if it were desirable to have unequal tendon forces (due to friction, or perhaps due to having tapered fingers) it would be possible to design the whiffle tree with correspondingly unequal bars.

Referring to Fig. 7 for notation, we can write expressions for the proximal and distal force balance using x_d and x_p to represent tangential displacement under load of the distal and proximal phalange respectively:

$$T_d \cos\theta_{t2} = F_{td} + x_d K_{lin} \cos\theta_{kd} \tag{4}$$

$$2T_p \cos\theta_{tp1} + x_d K_{lin} \cos\theta_{kp2} = T_d \cos\theta_{tp2} + x_p K_{lin} \cos\theta_{kp1} + F_{tp} \tag{5}$$

There is also a small frictional holding force across the pins of the proximal phalange that can be modeled with the Capstan equation. If the hand is actuated into position with a surplus of motor torque, the fingers are then loaded by contact with the surface being grasped, meaning that the distal tendon is the higher tension component and the proximal tendon has a slightly reduced load:

$$T_d = T_p e^{\mu(\theta_{tp1}+\theta_{tp2})} \tag{6}$$

If considering the opposite problem, when first starting to actuate the fingers, then T_d and T_p would be reversed.

Combining and rearranging equations 4 and 5 and substituting the aforementioned relationship between distal and proximal tendon tensions leads to an equation for the difference between the shear forces of the two phalanges, F_{tp} and F_{td}:

$$\begin{aligned} F_{tp} - F_{td} = T_p[&2\cos\theta_{tp1} \\ &- e^{\mu(\theta_{tp1}+\theta_{tp2})}(\cos\theta_{t2} + \cos\theta_{tp2})] \\ &+ K_{lin}[x_d \cos\theta_{kp2} - x_p \cos\theta_{kp1} \\ &+ x_d \cos\theta_{kd}] \end{aligned} \tag{7}$$

While the relationships among the various angular values will depend on the exact shape of the surface being contacted, in many low curvature cases there is not a significant difference in bending conditions between the two joints. Thus, $\theta_{tp1} \approx \theta_{tp2} \approx \theta_{t2} \approx \theta_t$ where θ_t is a generalized angular displacement of the tendons relative to the phalanges. Similarly, we can assume a generalized flexure spring force angle term $\theta_k \approx \theta_{kp1} \approx \theta_{kp2} \approx \theta_{kd}$. Additionally, the displacements x_p and x_d are not functions of specific geometry, but rather of the sliding distance until spine engagement prevents further motion. This means they are, instead, functions of surface roughness and will be roughly the same on most climbing holds for a given surface material, so that $x_p \approx x_d \approx x$. With these substitutions, a simplified relationship for the distal and proximal shear forces becomes:

$$F_{tp} - F_{td} = 2T_p \cos\theta_t (1 - e^{2\mu\theta_t}) + xK_{lin} \cos\theta_k \tag{8}$$

Several considerations emerge from these equations.

- Perfect load sharing occurs only if the finger is completely straight and there is zero displacement of the phalanges tangential to the surface being grasped, or if the two terms in eq. (8) cancel each other. Thus perfect load sharing can only be designed for a single surface curvature; however for moderate deviations from this shape the imbalance in forces will be small.

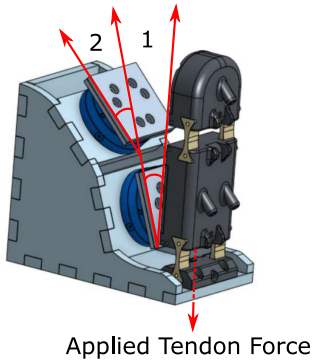

Fig. 8. Phalange load sharing test setup: blue cylinders denote the force/torque sensor locations; the square tiles mounted to the sensors were coated with sandpaper.

- Flexures should be soft so that they do not distort the force balance and the desired load sharing from the tendons persists.
- Load sharing is better at lower curvatures and gradually worsens as the fingers curl around a surface. The decreased performance in the latter situation is not a significant problem, however, because such situations allow for proportionally increased normal forces and are less reliant on the improved contact conditions provided by the spines.

IV. Validation

The mechanisms of load sharing and compliance outlined in Section III are the driving concepts behind the efficacy of this prototype, so testing focused on assessing these functional characteristics. Unfortunately, direct pull-out tests (i.e., inducing grasp failure) on rocky surfaces incur very high forces that can damage the spines and the 3D printed protoype (the final edition will be made from metal). Accordingly tests were conducted to ascertain the degree of load sharing achieved prior to failure, using rough but relatively weak surfaces that have been used in previous work on spines: roofing shingle and coarse, 60 grit sandpaper.

A. Phalange Load Sharing

A single finger test was designed to compare shear force values seen at the distal and proximal phalanges at different loads. Instrumented panels, with roofing shingle surfaces, were installed so that the proximal phalange made contact at 20° from vertical (angle 1 in Fig. 8) with the distal phalange rotated 25° with respect to the proximal. Contact forces were measured using an ATI Mini 45 force/torque sensor (1/16 N resolution) and tendon tensions were measured using a digital force gauge (Mark-10 Model M4-50, $0.1\,N$ resolution).

First, ideal load sharing was analyzed without flexures installed so that the phalanges were coupled only by the tendons. Non-ideal tests were then repeated with flexures installed. In both cases loads were applied equally to both tendons (as the design intended) or to only the distal tendon to confirm the predicted imbalance and approximate the case of typical underactuated hands.

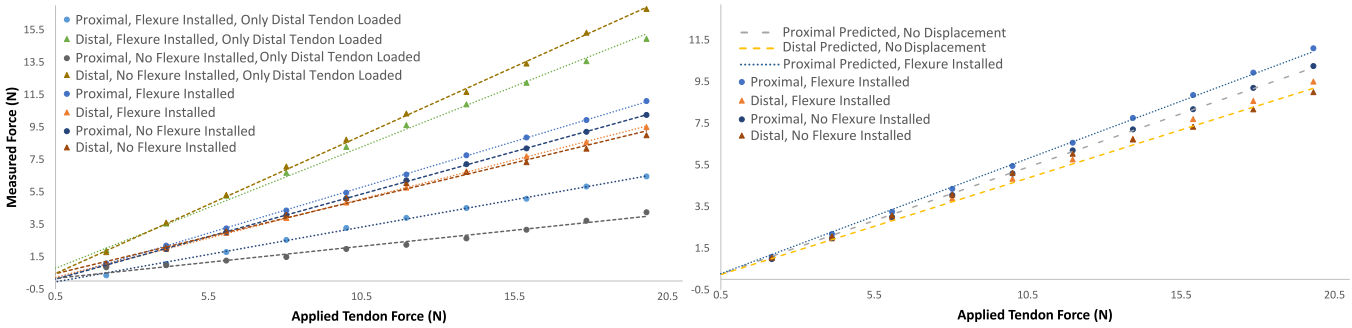

Fig. 9. (left) Measured tangential contact forces and best-fit lines, with and without elastic flexures installed. First four cases are when pulling only on the distal tendon; next four cases are with both tendons. (right) Comparison of measured forces (markers) with predicted values (lines) using eq. (8) – without flexures ("no displacement") or with flexures.

Figure 9 shows the four sets of results overlaid on each other. Triangular markers indicate results for the distal phalange, circular dots denote proximal data. Dashed lines are used for the no-flexure tests and dotted lines show results for the tests with flexures. The two outer pairs of lines are for loads applied only on the distal tendon; this leads to poor load sharing, as expected. The two inner pairs of lines show that with or without flexures, the measured tangential forces are approximately equal as the two tendons are loaded together by the whiffle tree mechanism. As expected, the match is slightly worse with flexures installed.

Additionally, to verify the force analysis presented in Section III-C, the measured load sharing results for the two-tendon loading cases are plotted alongside computed results using eq. (7), (8) in the right of Fig. 9. The calculated results generating the two lower lines are produced assuming a zero displacement condition, which is conceptually equivalent to the no-flexure test case, and matches that set of data well. Measured values of $\mu \approx 0.12$ were used for the Dyneema$^{\mathrm{TM}}$ tendon/steel frictional interface and $\theta_t \approx \theta_k \approx 12.5^\circ$ were used for the angles. For the case with flexures installed, the change in slope indicates that there is some, approximately linear correlation between applied force and displacement of the phalange rather than displacement being purely a function of spine/asperity contact properties. From the data, $x_d K_{lin} \approx 0.04 F_{applied}$ is a reasonable approximation of this effect, illustrated by the upper dotted blue line (Proximal Predicted, Flexure Installed).

In summary, the predictions match the measured values well for the no-flexure case and, with appropriate estimate of flexure stiffness, also match the data with flexures installed.

B. Palm Testing

First, a force vs. displacement test was performed on a single embedded spine unit to validate the accuracy of the FEA predictions of spine effective stiffness. An acrylic "asperity" was placed on the test spine unit and displaced until rotational failure occurred. Figure 10 shows the combined results of four tests fitted with a linear approximation. There is a slight trend towards hyperelastic behavior at maximum displacement, but the overall error of this estimate is low ($R^2 = 0.96$), indicating it is a reasonable estimate of $K_e \approx 2.4$ N/mm. Additionally, the average slip-off displacement of the spine (across the four trials where this occurred) was 3.73 ± 0.12 mm. These values are

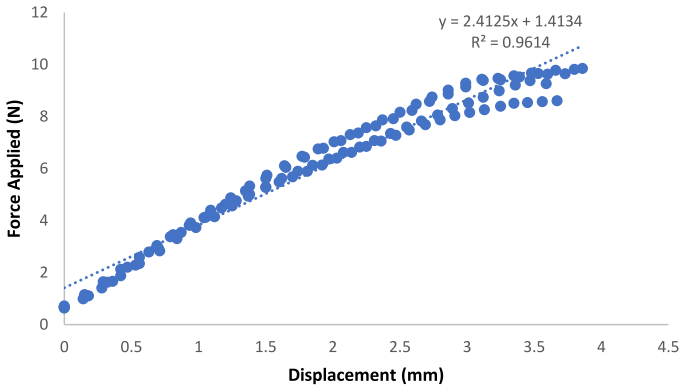

Fig. 10. Single spine unit force vs. displacement relationship.

very close to those predicted in Section III-A, and the expected failure force calculations can be updated to 3.6 N per spine and approximately 259 N for the entire palm.

These estimates give an upper bound on performance as they assume that every spine is loaded equally (i.e., each unit's performance is decoupled from its neighbors). In reality, load sharing is imperfect, so tests were performed to characterize the load sharing in the palm as a function of surface area and applied shear force. As in the previous test for the phalanges, pads of a rough material (roofing shingle) were mounted to an ATI mini force/torque sensor and brought into contact with the palm. First, a 5N force was applied to allow for spine engagement then vacuum was applied to the palm system to lock the particle jamming structure in place. Subsequently shear loads of 10 N, 15 N, and 20 N were applied to the palm. Each test was performed twice for two instrumented pads of various area ranging from 25 $\times$ 10 mm to 60 $\times$ 50 mm. Tests were then performed twice again with the tiles swapped to minimize the effects of any variability in the loading condition. For each loading case, we are interested in knowing whether the force at each instrumented pad area grows in proportion to the applied load and whether it maintains a ratio that would be expected with respect to the other pad, given the ratios of their areas.

Figure 11 provides a summary of the results. In the ideal case, each pad would produce a force that grows linearly with its area, and the force ratio between the two pads should match their area ratio. This case is represented by the upper yellow

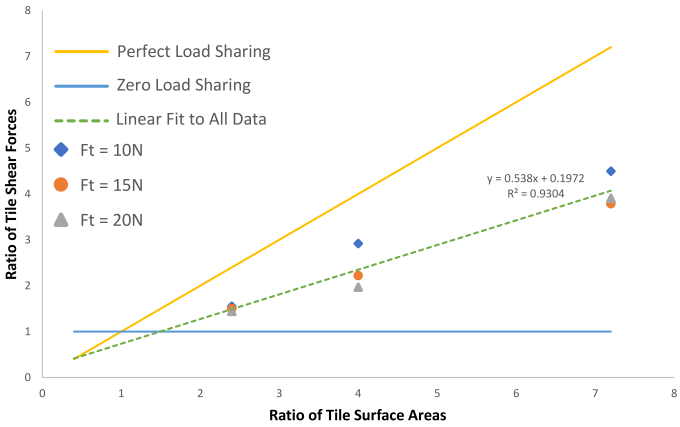

Fig. 11. Load sharing data for the particle jamming palm: each data point represents an average of four trials. Yellow line shows an ideal case where force grows linearly with area; blue line shows a worst case where force is independent of area.

line of unity slope. Conversely, a case with essentially no load sharing would be represented by the blue horizontal line – local force is independent of area.

The measured data show an approximately linear trend, in between the extremes of ideal and negligible load sharing, with a slope of 0.54. If we extrapolate this degree of load sharing to the entire palm we anticipate a maximum total shear force of 140 N on this structure alone which, although well below the predicted maximal value of 259 N, is enough to be effective. As discussed in Section V, there are several modifications we can make to increase this number.

As a final test, the palm was analyzed on a curved hold of approximately ellipsoidal shape with a minor radius in the vertical (climbing) direction of 0.15 m and a major radius in the horizontal direction of 0.4 m. The palm was engaged with the surface, vacuum was applied and tangential load was increased until slip-off. In this case slip-off occurs almost entirely due to rotation of the spines because the hold surface is tough and has strong asperities. The average maximum force at failure for 11 trials was 115.3 ± 18.6 N, indicating the calculated value of palm shear strength is a reasonable, but slightly high estimate of performance. The difference likely stems the different asperity densities of roofing shingle (used for calculations) and the climbing hold. We note also that while the absolute force is not high in comparison to the robot weight, it can easily be increased by increasing the number of spines and switching to stronger materials for the final prototype as described in Section V. Note also that with additional force provided by the fingers, and with any normal force against the surface, the tangential forces will be considerably higher.

V. Conclusions and Future Work

We have presented a soft and spiny end-effector, or paw, for a large legged robot that will enable it to climb steep rocky surfaces. The end-effector includes a particle-jamming palm to conform locally to wavy surfaces and under-actuated fingers to wrap partially around convex shapes. The contact surfaces of the palm and fingers are covered with spines to provide large shear forces with little normal force. However, for spines to work effectively in this design they must be integrated with the soft structures in a way that distributes the overall load over many spines. This is necessary (i) to prevent spine or spine/asperity contact failures and (ii) to prevent the spines from damaging the soft structures that contain them. The combination of these features allows the hand to successfully overload a 250 N force sensor on doubly curved rocky surfaces.

We present two new mechanisms to enable load sharing in this soft and spiny design. The first is a series of fingers, each of which is actuated by two tendons, connected to a whiffle tree differential mechanism. Using a single actuator, this solution provides equal forces on the tendons which, in turn, provide nearly equal tangential forces at proximal and distal contact areas for a range of curved surface geometries. Empirical results confirm the predicted ideal behavior with elastomeric flexures at the joints temporarily removed and nearly equal load sharing with the flexures installed.

The particle-jamming palm can conform to irregular surfaces and then lock its shape to provide moderate, but not ideal load sharing over the palm surface. One reason for the imperfect load sharing is that larger asperities, which can support higher loads, have a shorter lever arm for rotating the associated spines off of their respective asperities. This effect leads to variations in forces between spines, but is actually desirable for increasing the total shear force that can be supported by the palm. A model of individual spine performance is shown, scaled to the full palm, and validated.

Looking ahead, the final prototype will be made from stronger materials (metal for the phalanges and palm and a stronger, mesh-reinforced skin for the palm surface). With improved structural integrity, spine density can be increased $3\times$ in the palm, allowing higher shear forces as well as testing with some normal force, as will usually be the case when climbing. Field testing of the integrated prototype, including a standard climbing hook (as illustrated in Figs. 1 and 2) for crevice and ledge features, will take place on the RoboSimian platform.

Acknowledgment

The authors would like to thank the National Science foundation for funding support as well as Duke University, University of California Santa Barbara, and NASA Jet Propulsion Laboratory for their partnership.

References

[1] A. T. Asbeck, S. Kim, M. R. Cutkosky, W. R. Provancher, and M. Lanzetta, "Scaling hard vertical surfaces with compliant microspine arrays," *Int. J. Robot. Res.*, vol. 25, no. 12, pp. 1165–1179, 2006.

[2] M. J. Spenko *et al.*, "Biologically inspired climbing with a hexapedal robot," *J. Field Robot.*, vol. 25, pp. 223–242, 2008.

[3] K. A. Daltorio *et al.*, "Mini-whegs tm climbs steep surfaces using insect-inspired attachment mechanisms," *Int. J. Robot. Res.*, vol. 28, no. 2, pp. 285–302, 2009.

[4] G. C. Haynes *et al.*, "Rapid pole climbing with a quadrupedal robot," in *Proc. IEEE Int. Conf. Robot. Autom.*, 2009, pp. 2767–2772.

[5] A. Sintov, T. Avramovich, and A. Shapiro, "Design and motion planning of an autonomous climbing robot with claws," *Robot. Auton. Syst.*, vol. 59, no. 11, pp. 1008–1019, 2011.

[6] G. A. Lynch, J. E. Clark, P.-C. Lin, and D. E. Koditschek, "A bioinspired dynamical vertical climbing robot," *Int. J. Robot. Res.*, vol. 31, no. 8, pp. 974–996, 2012.
[7] T. L. Lam and Y. Xu, "Biologically inspired tree-climbing robot with continuum maneuvering mechanism," *J. Field Robot.*, vol. 29, no. 6, pp. 843–860, 2012.
[8] A. Parness *et al.*, "Gravity-independent rock-climbing robot and a sample acquisition tool with microspine grippers," *J. Field Robot.*, vol. 30, no. 6, pp. 897–915, 2013.
[9] A. Parness, K. C. Carpenter, and N. Wiltsie, "Terrain traversing device having a wheel with microhooks," U.S. Patent 8 978 807, Mar. 17, 2015.
[10] Y. Liu, S. Sun, X. Wu, and T. Mei, "A wheeled wall-climbing robot with bio-inspired spine mechanisms," *J. Bionic Eng.*, vol. 12, no. 1, pp. 17–28, 2015.
[11] J. S. Lee and R. S. Fearing, "Anisotropic collapsible leg spines for increased millirobot traction," in *Proc. IEEE Int. Conf. Robot. Autom.*, 2015, pp. 4547–4553.
[12] F. Xu, B. Wang, J. Shen, J. Hu, and G. Jiang, "Design and realization of the claw gripper system of a climbing robot," *J. Intell. Robot. Syst.*, vol. 89, pp. 1–17, 2017.
[13] A. Parness, N. Abcouwer, C. Fuller, N. Wiltsie, J. Nash, and B. Kennedy, "Lemur 3: A limbed climbing robot for extreme terrain mobility in space," in *Proc. IEEE Int. Conf. Robot. Autom*, 2017, pp. 5467–5473.
[14] A. Nishi, "Development of wall-climbing robots," *Comput. Elect. Eng.*, vol. 22, no. 2, pp. 123–149, 1996.
[15] S. Karumanchi *et al.*, "Team robosimian: Semiautonomous mobile manipulation at the 2015 darpa robotics challenge finals," *J. Field Robot.*, vol. 34, no. 2, pp. 305–332, 2016. [Online]. Available: https://onlinelibrary.wiley.com/doi/abs/10.1002/rob.21676
[16] M. R. Cutkosky and S. Kim, "Design and fabrication of multi-material structures for bioinspired robots," *Philos. Trans. Roy. Soc. London A: Math., Phys. Eng. Sci.*, vol. 367, no. 1894, pp. 1799–1813, 2009.
[17] A. C. Noel and D. L. Hu, "The tongue as a gripper," *J. Exp. Biol.*, vol. 221, no. 7, 2018, Art. no. jeb176289.
[18] S. Wang, H. Jiang, and M. R. Cutkosky, "Design and modeling of linearly-constrained compliant spines for human-scale locomotion on rocky surfaces," *Int. J. Robot. Res.*, vol. 36, no. 9, pp. 985–999, 2017. [Online]. Available: http://dx.doi.org/10.1177/0278364917720019
[19] S. Wang, "Traversing highly-varied terrain [electronic resource]: Enhanced contacts for human-scale robot locomotion," Ph.D. dissertation, Dept. Mech. Eng., Stanford Univ.,Stanford, CA, USA, 2017.
[20] L. Birglen, T. Laliberté, and C. Gosselin, *Underactuated Robotic Hands* (Springer Tracts in Advanced Robotics). vol. 40, Berlin Germany: Springer, 2008,
[21] G. A. Kragten and J. L. Herder, "The ability of underactuated hands to grasp and hold objects," *Mechanism Mach. Theory*, vol. 45, no. 3, pp. 408–425, 2010.
[22] J. Pons, R. Ceres, and F. Pfeiffer, "Multifingered dextrous robotics hand design and control: A review," *Robotica*, vol. 17, no. 6, pp. 661–674, 1999.
[23] S. Kim, C. Laschi, and B. Trimmer, "Soft robotics: A bioinspired evolution in robotics," *Trends Biotechnol.*, vol. 31, no. 5, pp. 287–294, 2013.
[24] D. Rus and M. T. Tolley, "Design, fabrication and control of soft robots," *Nature*, vol. 521, no. 7553, pp. 467–475, 2015.
[25] M. Manti, V. Cacucciolo, and M. Cianchetti, "Stiffening in soft robotics: A review of the state of the art," *IEEE Robot. Autom. Mag.*, vol. 23, no. 3, pp. 93–106, Sep. 2016.
[26] J. R. Amend, E. Brown, N. Rodenberg, H. M. Jaeger, and H. Lipson, "A positive pressure universal gripper based on the jamming of granular material," *IEEE Trans. Robot.*, vol. 28, no. 2, pp. 341–350, Apr. 2012.
[27] M. Cianchetti *et al.*, "Soft robotics technologies to address shortcomings in today's minimally invasive surgery: The stiff-flop approach," *Soft Robot.*, vol. 1, no. 2, pp. 122–131, 2014.
[28] Y. Wei *et al.*, "A novel, variable stiffness robotic gripper based on integrated soft actuating and particle jamming," *Soft Robot.*, vol. 3, no. 3, pp. 134–143, 2016.
[29] S. Wang, H. Jiang, and M. R. Cutkosky, "A palm for a rock climbing robot based on dense arrays of micro-spines," in *Proc. IEEE/RSJ Int. Conf. Intell. Robots Syst.*, 2016, pp. 52–59.
[30] H. Jiang, S. Wang, and M. R. Cutkosky, "Stochastic models of compliant spine arrays for rough surface grasping," *Int. J. Robot. Res.*, vol. 37, no. 7, pp. 669–687, 2018.
[31] J. M. Martn, V. L. D. Campo, M. L. Romn, J. M. G.-V. Horrillo, and J. S. G. Navarrete, "Description of the finger mechanical load of climbers of different levels during different hand grips in sport climbing," *J. Sports Sci.*, vol. 31, no. 15, pp. 1713–1721, 2013. [Online]. Available: http://dx.doi.org/10.1080/02640414.2013.797592